

# Biobased Acrylate Photocurable Resin Formulation for Stereolithography 3D Printing

Vincent S. D. Voet,<sup>\*,†,Ⓜ</sup> Tobias Strating,<sup>‡</sup> Geraldine H. M. Schnelting,<sup>†</sup> Peter Dijkstra,<sup>§,||</sup> Martin Tietema,<sup>§</sup> Jin Xu,<sup>||</sup> Albert J. J. Woortman,<sup>||</sup> Katja Loos,<sup>||,Ⓜ</sup> Jan Jager,<sup>†</sup> and Rudy Folkersma<sup>†</sup>

<sup>†</sup>Professorship Sustainable Polymers, NHL Stenden University of Applied Sciences, van Schaikweg 94, 7811 KL Emmen, Leeuwarden, The Netherlands

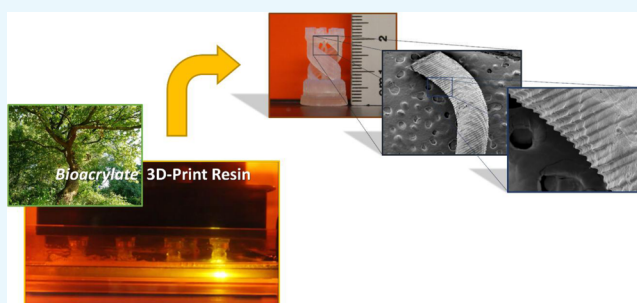
<sup>‡</sup>SymbioShape Research and Development, SymbioShape, Agora 4, 8934 CJ Leeuwarden, The Netherlands

<sup>§</sup>KNN Bioplastic, KNN Groep, Duinkerkenstraat 13, 9723 BN Groningen, The Netherlands

<sup>||</sup>Macromolecular Chemistry and New Polymeric Materials, Zernike Institute for Advanced Materials, University of Groningen, Nijenborgh 4, 9747 AG Groningen, The Netherlands

## Supporting Information

**ABSTRACT:** To facilitate the ongoing transition toward a circular economy, the availability of renewable materials for additive manufacturing becomes increasingly important. Here, we report the successful fabrication of complex shaped prototypes from biobased acrylate photopolymer resins, employing a commercial stereolithography apparatus (SLA) 3D printer. Four distinct resins with a biobased content ranging from 34 to 67% have been developed. All formulations demonstrated adequate viscosity and were readily polymerizable by the UV-laser-based SLA process. Increasing the double-bond concentration within the resin results in stiff and thermally resilient 3D printed products. High-viscosity resins lead to high-resolution prototypes with a complex microarchitecture and excellent surface finishing, comparable to commercial nonrenewable resins. These advances can facilitate the wide application of biobased resins for construction of new sustainable products via stereolithographic 3D printing methods.



## INTRODUCTION

Additive manufacturing or 3D printing offers design freedom, efficient product development, and on-demand production. Mass fabrication and global logistics of both raw materials and products are not needed; 3D printing only requires local logistics of raw materials and 3D printers in close proximity. Biomaterials are produced from renewable resources, such as organic biomass, instead of fossil fuels, and can therefore reduce the environmental impact of additive manufacturing. Hence, the use of renewable materials for 3D printing enables local manufacturing of new innovative and sustainable products. Ultimately, this provides the opportunity to realize a biobased and circular economy, which is restorative and regenerative by design.<sup>1</sup>

Currently, a variety of 3D printing technologies are available, allowing the efficient production of three-dimensional physical objects from digital models via layer-by-layer addition of materials. Fused deposition modeling (FDM) is a low-cost rapid prototyping process based on the extrusion of thermoplastic filaments and the deposition of molten materials onto a stage. The use of biobased polymers such as polylactic acid (PLA) in monofilaments has gained a lot of attention because of their unique properties for 3D printing combined with their renewability and biocompatibility.<sup>2</sup> In addition, life cycle

analysis has demonstrated that the energy demand of manufacturing polymer products can be reduced up to 64% when applying low-cost FDM printing with PLA.<sup>3</sup>

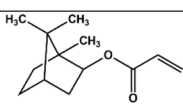
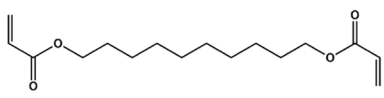
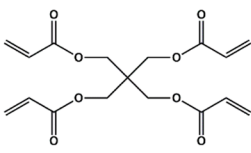
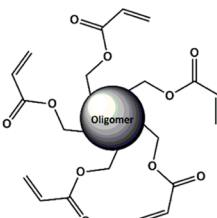
Although FDM is the most widely used rapid prototyping technique, additive manufacturing started in the 1980s with the development of the stereolithography apparatus (SLA) by Hull at 3D Systems.<sup>4,5</sup> SLA relies on layer-by-layer curing and solidification of liquid photopolymer resins by a UV laser. When a light projector is applied instead, exposing the entire layer to UV light simultaneously, the process is named digital light processing (DLP). Additive manufacturing via SLA or DLP process is applicable for high-resolution prototyping and fabrication of (bio)medical devices, for example, dental implants<sup>6</sup> and patient-specific scaffolds for tissue regeneration.<sup>7</sup> Despite the fast processing, excellent surface finishing, and extremely high feature resolution (5–50 μm), postcuring of printed objects is required to guarantee the conversion of any unreacted groups.<sup>8</sup> Moreover, current commercialized photopolymer resins are expensive and fossil-based, thus non-renewable.<sup>2,5</sup>

Received: October 26, 2017

Accepted: December 21, 2017

Published: February 2, 2018

Table 1. Characteristics of Biobased Acrylate Monomers and Oligomers

Acrylate	Structural formula	BC %	$f$	$\rho$ kg·dm <sup>-3</sup>	$M$ kg·mol <sup>-1</sup>	$[C=C]_0^a$ mol·dm <sup>-3</sup>	$\eta$ Pa·s
SA5102		75	1	0.99	0.21	4.8	0.01
SA5201		60	2	0.98	0.28	7.0	0.01
SA5400		10	4	1.17	0.35	13	0.35
SA7101		70	5	1.04	1.7	2.7	17

<sup>a</sup>Double-bond concentrations are calculated according to the following equation:  $[C=C]_0 = f \cdot \rho / M$ .

SLA/DLP resins require photocurable moieties, typically multifunctional epoxy or (meth)acrylate monomers, to ensure cross-linking. Epoxy resins are cured in a step-growth manner in the presence of amines or anhydrides, whereas acrylate monomers generally undergo radical chain-growth polymerization.<sup>9</sup> Typical acrylate photoresins consist of a combination of (multi)functional monomers, oligomers, a photoinitiator, and an optical absorber.<sup>10</sup> The absorber function is to control the penetration depth of the incident light and therefore the polymerization. The mechanical behavior of thermosetting polymers is closely related to the underlying molecular architecture, which is dependent on the monomer composition, photoinitiator concentration, and curing conditions. High cross-link densities result in increased stiffness and high thermal stability, whereas toughness decreases. Indeed, despite their rapid curing and good spatial resolution, acrylate systems commonly show low toughness and tend to be brittle because of their high cross-link density and inhomogeneous architecture.<sup>5,9</sup>

In recent years, a limited number of biodegradable photopolymer resins have been developed and applied in stereolithography printing.<sup>11,12</sup> This concept was initially reported by Matsuda et al., who developed copolymers of trimethylene carbonate and poly( $\epsilon$ -caprolactone) that were used to fabricate biodegradable stereolithographic microstructures.<sup>13,14</sup> Photo-cross-linkable poly(propylene fumarate) is applied in the SLA to construct complex 3D scaffolds for bone tissue engineering applications.<sup>15</sup> Porous network scaffolds with a gyroid architecture were accurately fabricated by photo-cross-linking of biodegradable poly(D,L-lactide) macromonomers functionalized with methacrylate end groups.<sup>16</sup>

The availability of biobased photocurable resins, produced from renewable resources, is even more scarce.<sup>17</sup> Microscaffolds were prepared by stereolithography using biobased unsaturated polyesters,<sup>18</sup> using styrene or hydroxyethyl methacrylate as a

cross-linking agent. Very recently, Miao and co-workers utilized soybean oil epoxidized acrylate as a biocompatible and renewable liquid resin for SLA, and the solidified resin possesses striking shape memory effects.<sup>19</sup> Nevertheless, both resin systems were not tested on a commercial 3D printing apparatus. To facilitate the ongoing transition from an economy based on fossil fuels to a biobased economy, the availability of cost-competitive sustainable materials for rapid prototyping becomes increasingly important. Hence, this paper will discuss the straightforward formulation of novel biobased acrylate resins for stereolithography 3D printing and their performance in comparison to commercial counterparts.

## EXPERIMENTAL SECTION

**Materials.** Isobornyl acrylate (SA5102, Sartomer), 1,10-decanediol diacrylate (SA5201, Sartomer), pentaerythritol tetraacrylate (SA5400, Sartomer), and multifunctional acrylate oligomer (SA7101, Sartomer,  $M_n = 1.7$  kg·mol<sup>-1</sup>) were kindly supplied by Sartomer (Arkema Group). Table 1 depicts the characteristics of the bioacrylates, such as their biobased carbon content (BC), acrylate functionality ( $f$ ), molecular weight ( $M$ ), density ( $\rho$ ), concentration of double bonds ( $[C=C]_0$ ), and viscosity ( $\eta$ ). The molecular weight of the multifunctional acrylate oligomer was determined by gel permeation chromatography (GPC) (Figure S1). Diphenyl(2,4,6-trimethylbenzoyl)phosphine oxide (TPO, Aldrich, 97%) and 2,5-bis(5-*tert*-butyl-benzoxazol-2-yl)thiophene (BBOT, Aldrich, 99%) were used as received and employed as an initiator and an optical absorber, respectively. For comparison, commercially available Autodesk Standard Clear Prototyping resin (ACPR-48, Autodesk) was acquired.

**Resin Preparation.** A typical photocurable resin was prepared as follows. A TPO initiator (0.40 w/w %) and a BBOT absorber (0.16 w/w %) were added to a cylindrical polypropylene flask in a darkened fume hood and dissolved in an SA5102 acrylate monomer (19.9 w/w %) by vigorous

Table 2. Compositions<sup>a</sup> and Characteristics of BAPRs

resin	SAS102 (w/w %)	SAS201 (w/w %)	SAS400 (w/w %)	SA7101 (w/w %)	BC (%)	[C=C] <sub>0</sub> (mol·dm <sup>-3</sup> )	$\eta^b$ (Pa·s)	E (MPa)	$\sigma_m$ (MPa)
BAPR- $\alpha$	20	40		40	67	4.9	0.15	64.8 ± 2.8	2.6 ± 0.2
BAPR- $\beta$		60		40	64	5.3	0.14	159 ± 8.8	4.0 ± 0.2
BAPR- $\gamma$		20	40	40	44	7.5	0.99	364 ± 21	3.0 ± 0.2
BAPR- $\delta$			60	40	34	8.7	4.6	383 ± 13	7.0 ± 0.8
ACPR-48							0.44	836 ± 44	19 ± 2.3

<sup>a</sup>0.40 w/w % TPO initiator; 0.16 w/w % BBOT absorber. <sup>b</sup>Viscosity at a shear rate of 100 s<sup>-1</sup>.

stirring. Subsequently, the SAS201 acrylate monomer (39.8 w/w %) and SA7101 acrylate oligomer (39.8 w/w %) were added. The resulting biobased acrylate photopolymer resin (BAPR- $\alpha$ ) was stirred for 10 min to ensure homogeneity, and the flask was closed by a screw cap.

**Stereolithographic 3D Printing.** Prior to printing, digital models were downloaded from the web as a standard tessellation language file from open source sites<sup>20,21</sup> and subsequently processed with PreForm (Formlabs) and Print Studio (Autodesk) software, which enables the orientation of the objects on the 3D build platform.

An Autodesk Ember (desktop DLP) 3D printer was employed to cure the commercial (ACPR) resin and build various 3D products. The printer used an LED projector ( $\lambda = 405$  nm, 5 W) and had a building volume of 64 × 40 × 134 mm<sup>3</sup>. Stereolithographic printing was performed according to the preprogrammed Standard Clear settings at room temperature, and a layer thickness of 50  $\mu$ m was selected. Tensile bars (ISO 527-2-1BA) were printed normal to the build direction because of the limited building volume.

A Formlabs Form 2 (desktop SLA) 3D printer was employed to cure BAPR and commercial ACPR and build various 3D products. The printer used a class-1 laser ( $\lambda = 405$  nm, 250 mW) with a laser spot size of 140  $\mu$ m and had a building volume of 145 × 145 × 175 mm<sup>3</sup>. Stereolithographic printing was performed according to the preprogrammed Clear V2 settings in open modus at room temperature, and a layer thickness of 50  $\mu$ m was selected. Tensile bars (ISO 527-2-1BA) were printed normal to the build direction (Figure S2). Complex shaped prototypes with a rook tower design (Figure S3) were produced for optical analysis.

After the printing procedure, the products were removed from the printing head and soaked for 10 min in an alcohol bath containing isopropanol (IPA, Höfer Chemie, 99.9%) to remove any unreacted resin. The rinsing procedure of 10 min was repeated in a second IPA bath. Afterward, the products were exposed to UV irradiation in a self-fabricated UV oven ( $\lambda = 365$  nm, 36 W) for 60 min at room temperature to ensure complete curing.

**Characterization.** GPC was performed in dimethylformamide (1 mL min<sup>-1</sup>) with 0.01 N LiBr on a Viscotek GPCmax equipped with model 302 TDA detectors, using two columns (Agilent, PolarGel L + M, particle size 8  $\mu$ m, 7.5 × 300 mm<sup>2</sup>). Molecular weights were calculated relative to poly(methyl methacrylate) according to universal calibration using narrow disperse standards (Polymer Laboratories).

A Paar Physica MCR300 rheometer with a parallel-plate geometry was used to measure the resin viscosity. The diameter of the geometry was 50 mm, and the gap between two geometries was 1 mm. All measurements were performed at room temperature.

Fourier transform infrared (FTIR) spectroscopy was performed in the attenuated total reflection (ATR) mode using a Bruker A225/QHP Platinum-ATR accessory with a diamond top plate on a Bruker VERTEX 70 spectrometer equipped with a DLaTGS detector at a resolution of 2 cm<sup>-1</sup>.

Thermogravimetric analysis (TGA) was performed on a PerkinElmer thermogravimetric analyzer TGA 7. A temperature range of 25–700 °C was applied at a heating scan rate of 10 °C/min under a nitrogen atmosphere.

An Instron 4301 1kN series IX was used to determine the mechanical properties, such as tensile strength and Young's modulus. Measurements were performed in quintuplicate at room temperature and according to the ISO 527 method at a crosshead speed of 5 mm/min.

Scanning electron microscopy (SEM) was carried out on a Philips XL30 ESEM-FEG operated at an accelerating voltage of 5 kV. Prior to imaging, the specimens were coated with 30 nm Pt/Pd (80:20).

## RESULTS AND DISCUSSION

**Resin Formulations.** Homogeneous acrylate photoresins with varying BC were successfully prepared. The open-source ACPR-48 from Autodesk's Ember 3D printing project was acquired as a reference.<sup>22</sup> Mimicking the composition of ACPR-48, BAPR- $\alpha$  consists of 20 w/w % monofunctional reactive diluent (i.e., isobornyl acrylate), 40 w/w % difunctional monomer (i.e., 1,10-decanediol diacrylate), 40 w/w % multifunctional acrylate oligomer, 0.40 w/w % initiator, and 0.16 w/w % optical absorber. This formulation leads to an average biobased content of 67%, calculated from the individual BC of the components (Table 1). The compositions of BAPR- $\beta$ , BAPR- $\gamma$ , and BAPR- $\delta$  are depicted in Table 2. With low-cost biobased acrylates as the main component, the BAPR resins are extremely cost-competitive with respect to commercial products.

For the application in a stereolithographic layer-by-layer printing process, the resin viscosity is a crucial parameter. In general, low viscosities are desired to allow appropriate recoating of the liquid resin between the last layer of the model and the resin tank surface.<sup>23</sup> The viscosity of the uncured bioacrylate resins was determined as a function of shear rate (Figure 1), and Newtonian behavior was observed in all samples. Table 2 displays the viscosities at a high shear rate of 100 s<sup>-1</sup>, which is commonly achieved during the recoating step of the process.<sup>24</sup> BAPR- $\alpha$  and BAPR- $\beta$  have a lower viscosity in comparison to ACPR-48. BAPR- $\gamma$  and especially BAPR- $\delta$  demonstrate higher viscosities because of the incorporation of more viscous pentaerythritol tetraacrylate (Table 1). Nevertheless, both values are on the same order of those of other commercial photocurable resins of Formlabs; Formlabs' clear and flexible resins have viscosities of 1.6 and 7.3 Pa·s, respectively (Figure S4). All formulations developed in this

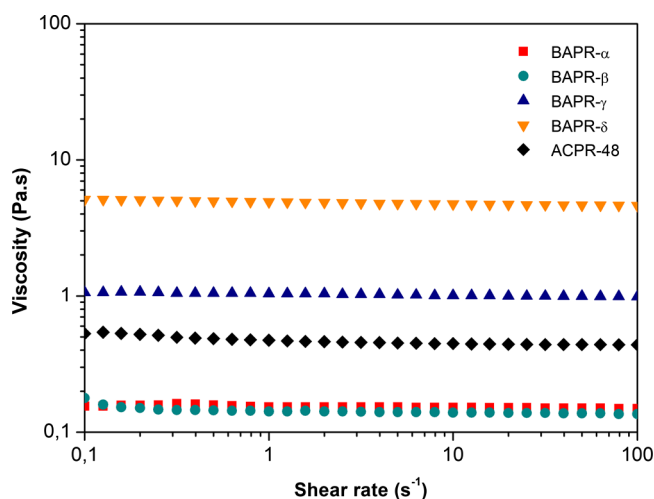


**Figure 1.** Viscosity as a function of shear rate for uncured BAPR samples and commercial ACPR-48.

study demonstrate adequate viscosity for the application in the stereolithographic printing equipment.

### Stereolithographic 3D Printing of Bioacrylate Resins.

Both SLA and DLP processes were applied, employing Formlabs Form 2 and Autodesk Ember 3D printers, respectively, to build 3D constructs. In general, laser-based SLA is more precise and suitable for the fabrication of high-resolution structures, whereas DLP is faster. To explore and compare both techniques, the mechanical properties of cured ACPR-48 were addressed. Consequently, tensile bars were printed on both 3D printers and subsequently analyzed with stress–strain measurements. No significant difference was observed between SLA and DLP in terms of tensile strength ( $\sigma_m$ ) (Figure 2). In addition, similar values for the elastic

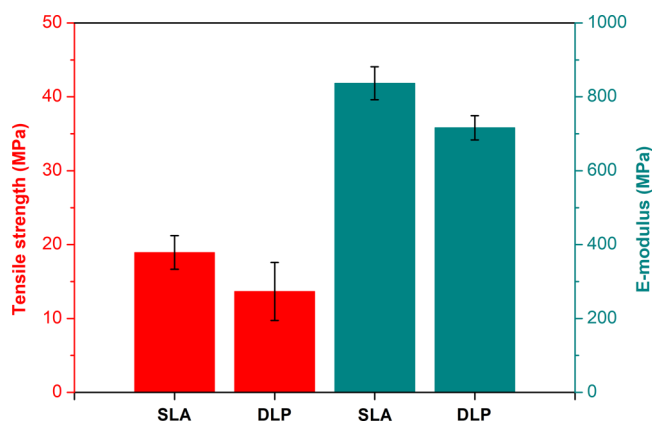


**Figure 2.** Tensile strength (red) and Young's modulus (cyan) of cured ACPR-48 printed on both Formlabs Form 2 SLA 3D printer and Autodesk Ember DLP 3D printer. The tensile bars (ISO 527-2-1BA) were printed normal to the build direction.

modulus ( $E$ ) were determined for both techniques. Because the mechanical performance of the commercial resin is rather independent on the printing method, all bioacrylate resins were cured on the Form 2 SLA printer because of the limited building volume of the Ember DLP printer.

The successful polymerization of BAPR- $\alpha$  is confirmed by postprinting FTIR analysis (Figure 3). The signals corresponding to C=C bonds in the acrylate moiety (1627, 1407, and 806

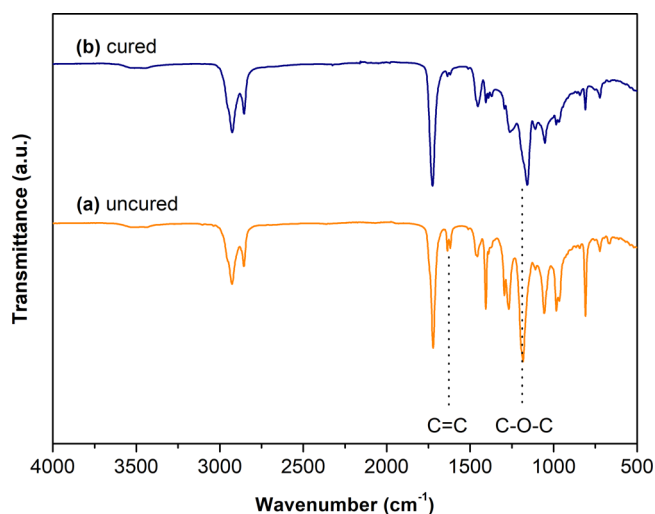


**Figure 3.** FTIR spectra of (a) uncured BAPR- $\alpha$  (orange) and (b) cured BAPR- $\alpha$  (blue) printed on the Formlabs Form 2 SLA 3D printer.

$\text{cm}^{-1}$ ) significantly decreased after printing, indicating the consumption of double bonds due to the network formation. For the same reason, the signal representing to C–O–C oscillation of the ester group shifted from 1188 to 1156  $\text{cm}^{-1}$ .

All BAPRs ( $\alpha$ – $\delta$ ) were successfully applied in the stereolithographic 3D printing process for the construction of tensile bars and complex shaped prototypes, enabling a thorough mechanical and optical characterization, respectively. Despite successful printing, BAPR- $\alpha$  causes the swelling of the polydimethylsiloxane (PDMS) layer inside the SLA vat, thereby destructing the resin tray within a few days. By removing isobornyl acrylate as a monofunctional component from the bioacrylate resin formulation, the swelling of PDMS was prevented. As a result, BAPR- $\beta$ , BAPR- $\gamma$ , and BAPR- $\delta$  remained stable in their SLA trays for months.

**Mechanical Performance.** The nature of a polymeric network, that is, the molecular architecture, strongly influences the mechanical behavior of the bulk material.<sup>9,25</sup> The cross-link density particularly dictates the strength and modulus of a thermoset. In general, a higher concentration of double bonds ( $[C=C]_0$ ) in the system results in the formation of a highly cross-linked polymer network,<sup>26,27</sup> and higher cross-link densities lead to an increased stiffness of the material. Indeed, the Young's modulus ( $E$ ) of the cured BAPR products increases with increasing double-bond concentration (Table 2). The same trend is observed with thermal analysis. TGA curves in Figure 4 indicate an increased thermal stability with increasing  $[C=C]_0$ . The lower cross-link densities in cured BAPR- $\alpha$  and BAPR- $\beta$  systems lead to polymer degradation at lower temperatures in comparison to BAPR- $\gamma$  and BAPR- $\delta$ .

The mechanical performance of the cured BAPR- $\delta$  was the highest with respect to all biobased resins, demonstrating an ultimate tensile strength of 7.0 MPa (Table 2). Nevertheless, the tensile strength of the cured ACPR-48 is 2.7 times higher. The thermal stability of the commercial product, however, is lower with respect to those of both BAPR- $\gamma$  and BAPR- $\delta$  (Figure 4).

**Morphology.** The construction of complex shaped prototypes was performed for optical analysis. Prototypes with a rook tower design were successfully printed for all biobased acrylate resins, which are demonstrated by the

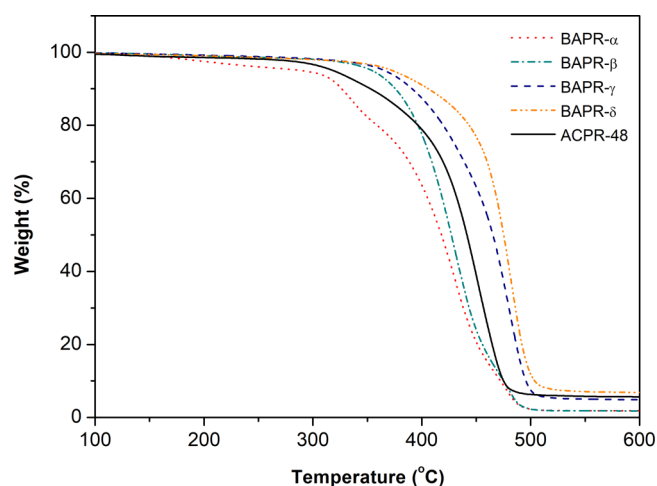


**Figure 4.** TGA curves of the cured BAPR samples and commercial ACPR-48 printed on the Formlabs Form 2 SLA 3D printer.

photographs in Figure 5. The SEM images of the internal helix part, having a diameter of ca.  $700\ \mu\text{m}$ , reveal a high feature resolution and excellent surface finishing and confirm the potential of our bioacrylate resins to fabricate 3D structures with complex microarchitectures. The electron micrographs at a high magnification demonstrate serration at the vertical edges of the internal helix in all samples, which is typical for the SLA/DLP process. This is caused by the top surface of exposed ( $50\ \mu\text{m}$ ) layers receiving a larger dose of UV radiation than the back surface.<sup>10</sup>

Extensive cracks are observed both macroscopically and microscopically in the prototypes built from BAPR- $\alpha$  and BAPR- $\beta$  (Figure 5a,b). Cracking in UV-cured systems can result from shrinkage forces developed during and after curing.<sup>9</sup> For (meth)acrylated systems, shrinkage is found to be inversely related to the initial viscosity.<sup>28,29</sup> As a result, this behavior is significantly reduced when curing more viscous BAPR- $\gamma$ . The SEM images only reveal minor cracks at the surface (Figure 5c), indicating less shrinkage. Finally, the prototypes fabricated with highly viscous BAPR- $\delta$  demonstrate a very smooth surface (Figure 5d), equivalent to that fabricated with the commercial standard (Figure 5e).

## CONCLUSIONS

Renewable photopolymer resins based on biobased acrylates are prepared for the application in stereolithographic 3D printing. Their resin viscosities of  $0.14\text{--}4.6\ \text{Pa}\cdot\text{s}$  are within the range of current commercial counterparts, and the use of low-cost bioacrylates makes the resins potentially cost-competitive. Straightforward application of the bioresin formulations in a commercial SLA printer is demonstrated by the successful fabrication of tensile bars and prototypes with a complex rook tower design. The elastic modulus and thermostability of the cured products increased with increasing double-bond concentration, corresponding to a higher degree of cross-linking. Cracking as a result of shrinkage stress is strongly reduced for more viscous resins, leading to complex shaped prototypes with high feature resolution and excellent surface finishing. This progress enables on-demand fabrication of a wide range of sustainable and renewable products and facilitates the biobased economy.

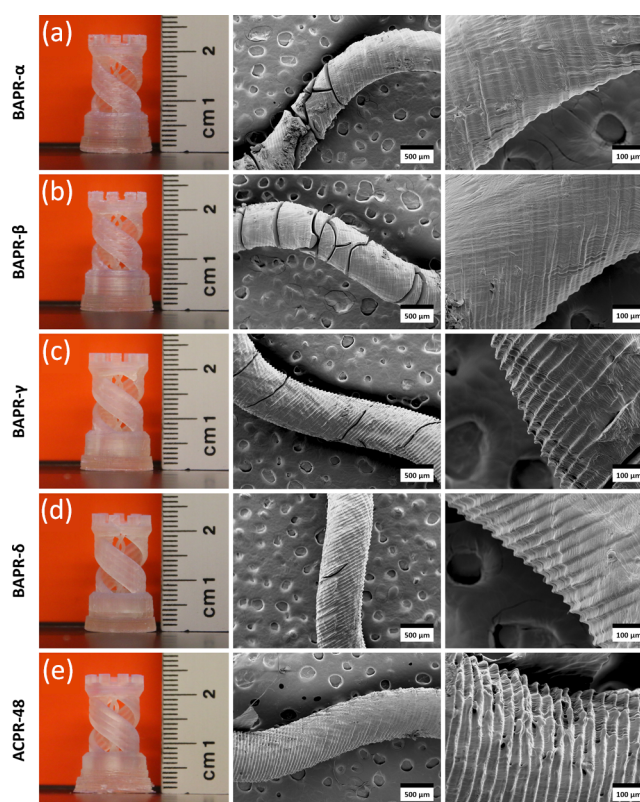


**Figure 5.** (a) Photograph of the rook tower prototype printed with BAPR- $\alpha$  (left) and corresponding SEM images of the internal helix in the prototype (right), (b) photograph of the rook tower prototype printed with BAPR- $\beta$  (left) and corresponding SEM images of the internal helix in the prototype (right), (c) photograph of the rook tower prototype printed with BAPR- $\gamma$  (left) and corresponding SEM images of the internal helix in the prototype (right), (d) photograph of the rook tower prototype printed with BAPR- $\delta$  (left) and corresponding SEM images of the internal helix in the prototype (right), and (e) photograph of the rook tower prototype printed with ACPR-48 (left) and corresponding SEM images of the internal helix in the prototype (right). All products were printed on the Formlabs Form 2 SLA 3D printer.

## ASSOCIATED CONTENT

### Supporting Information

The Supporting Information is available free of charge on the ACS Publications website at DOI: 10.1021/acsomega.7b01648.

Additional GPC results, object design, and rheological data (PDF)

## AUTHOR INFORMATION

### Corresponding Author

\*E-mail: vincent.voet@stenden.com (V.S.D.V.).

### ORCID

Vincent S. D. Voet: 0000-0003-0863-0616

Katja Loos: 0000-0002-4613-1159

### Notes

The authors declare no competing financial interest.

## ACKNOWLEDGMENTS

This study was funded by the Dutch Ministry of Economic Affairs, the Northern Netherlands Provinces Alliance (SNN), and the Province of Friesland via a Fryslân Fernijt IV subsidy.

In addition, the study was supported by the Netherlands Organization for Scientific Research (NWO) via a VICI innovational research grant. Jur van Dijken is kindly acknowledged for TGA measurements. The authors thank Harm-Jan Bouwers for valuable feedback.

## REFERENCES

- (1) van Wijk, A.; van Wijk, I. *3D Printing with Biomaterials: Towards a Sustainable and Circular Economy*; IOS Press: Amsterdam, 2015.
- (2) Bhatia, S. K.; Ramadurai, K. W. *3D Printing and Bio-Based Materials in Global Health*; Springer: Cham, 2017.
- (3) Kreiger, M.; Pearce, J. M. Environmental Life Cycle Analysis of Distributed Three-Dimensional Printing and Conventional Manufacturing of Polymer Products. *ACS Sustainable Chem. Eng.* **2013**, *1*, 1511–1519.
- (4) Hull, C. W. Apparatus for production of three-dimensional objects by stereolithography. U.S. Patent 4,575,330, 1986.
- (5) Gross, B. C.; Erkal, J. L.; Lockwood, S. Y.; Chen, C.; Spence, D. M. Evaluation of 3D Printing and Its Potential Impact on Biotechnology and the Chemical Sciences. *Anal. Chem.* **2014**, *86*, 3240–3253.
- (6) van Noort, R. The future of dental devices is digital. *Dent. Mater.* **2012**, *28*, 3–12.
- (7) Chia, H. N.; Wu, B. M. Recent advances in 3D printing of biomaterials. *J. Biol. Eng.* **2015**, *9*, 4.
- (8) Oskui, S. M.; Diamante, G.; Liao, C.; Shi, W.; Gan, J.; Schlenk, D.; Grover, W. H. Assessing and Reducing the Toxicity of 3D-Printed Parts. *Environ. Sci. Technol. Lett.* **2016**, *3*, 1–6.
- (9) Ligon-Auer, S. C.; Schwentenwein, M.; Gorsche, C.; Stampfl, J.; Liska, R. Toughening of photo-curable polymer networks: a review. *Polym. Chem.* **2016**, *7*, 257–286.
- (10) Gong, H.; Beauchamp, M.; Perry, S.; Woolley, A. T.; Nordin, G. P. Optical approach to resin formulation for 3D printed microfluidics. *RSC Adv.* **2015**, *5*, 106621–106632.
- (11) Melchels, F. P. W.; Feijen, J.; Grijpma, D. W. A review on stereolithography and its applications in biomedical engineering. *Biomaterials* **2010**, *31*, 6121–6130.
- (12) Skoog, S. A.; Goering, P. L.; Narayan, R. J. Stereolithography in tissue engineering. *J. Mater. Sci.: Mater. Med.* **2014**, *25*, 845–856.
- (13) Matsuda, T.; Mizutani, M.; Arnold, S. C. Molecular Design of Photocurable Liquid Biodegradable Copolymers. I. Synthesis and Photocuring Characteristics. *Macromolecules* **2000**, *33*, 795–800.
- (14) Matsuda, T.; Mizutani, M. Liquid acrylate-endcapped biodegradable poly( $\epsilon$ -caprolactone-co-trimethylene carbonate). II. Computer-aided stereolithographic microarchitectural surface photo-constructs. *J. Biomed. Mater. Res.* **2002**, *62*, 395–403.
- (15) Lee, K.-W.; Wang, S.; Fox, B. C.; Ritman, E. L.; Yaszemski, M. J.; Lu, L. Poly(propylene fumarate) Bone Tissue Engineering Scaffold Fabrication Using Stereolithography: Effects of Resin Formulations and Laser Parameters. *Biomacromolecules* **2007**, *8*, 1077–1084.
- (16) Melchels, F. P. W.; Feijen, J.; Grijpma, D. W. A poly(D,L-lactide) resin for the preparation of tissue engineering scaffolds by stereolithography. *Biomaterials* **2009**, *30*, 3801–3809.
- (17) Skliutas, E.; Kašėtaitė, S.; Grigalevičiūtė, G.; Jonušauskas, L.; Rekštytė, S.; Ostrauskaitė, J.; Malinauskas, M. Bioresists from renewable resources as sustainable photoresins for 3D laser micro-lithography: material synthesis, cross-linking rate and characterization of the structures. *Proc. SPIE* **2017**, *10115*, 11.
- (18) Gonçalves, F. A. M. M.; Costa, C. S. M. F.; Fabela, I. G. P.; Farinha, D.; Faneca, H.; Simões, P. N.; Serra, A. C.; Bártolo, P. J.; Coelho, J. F. J. 3D printing of new biobased unsaturated polyesters by microstereo-thermallithography. *Biofabrication* **2014**, *6*, 035024.
- (19) Miao, S.; Zhu, W.; Castro, N. J.; Nowicki, M.; Zhou, X.; Cui, H.; Fisher, J. P.; Zhang, L. G. 4D printing smart biomedical scaffolds with novel soybean oil epoxidized acrylate. *Sci. Rep.* **2016**, *6*, 27226.
- (20) Pearce, J. M. Building Research Equipment with Free, Open-Source Hardware. *Science* **2012**, *337*, 1303.
- (21) Thingiverse—Digital Designs for Physical Objects. <https://www.thingiverse.com> (accessed June 2017).
- (22) Adzima, B. The Ember Printer: An Open Platform for Software, Hardware and Materials Development. *Uv.eb West Conference*: Redondo Beach, CA, 2015.
- (23) Weng, Z.; Zhou, Y.; Lin, W.; Senthil, T.; Wu, L. Structure-property relationship of nano enhanced stereolithography resin for desktop SLA 3D printer. *Composites, Part A* **2016**, *88*, 234–242.
- (24) Scalera, F.; Corcione, C. E.; Montagna, F.; Sannino, A.; Maffezzoli, A. Development and characterization of UV curable epoxy/hydroxyapatite suspensions for stereolithography applied to bone tissue engineering. *Ceram. Int.* **2014**, *40*, 15455–15462.
- (25) Elliott, J.; Bowman, C. Predicting network formation of free radical polymerization of multifunctional monomers. *Polym. React. Eng.* **2002**, *10*, 1–19.
- (26) Anseth, K. S.; Goodner, M. D.; Reil, M. A.; Kannurpatti, A. R.; Newman, S. M.; Bowman, C. N. The Influence of Comonomer Composition on Dimethacrylate Resin Properties for Dental Composites. *J. Dent. Res.* **1996**, *75*, 1607–1612.
- (27) Muggli, D. S.; Burkoth, A. K.; Anseth, K. S. Crosslinked polyanhydrides for use in orthopedic applications: Degradation behavior and mechanics. *J. Biomed. Mater. Res.* **1999**, *46*, 271–278.
- (28) Ellakwa, A.; Cho, N.; Lee, I. B. The effect of resin matrix composition on the polymerization shrinkage and rheological properties of experimental dental composites. *Dent. Mater.* **2007**, *23*, 1229–1235.
- (29) Charton, C.; Falk, V.; Marchal, P.; Pla, F.; Colon, P. Influence of T<sub>g</sub>, viscosity and chemical structure of monomers on shrinkage stress in light-cured dimethacrylate-based dental resins. *Dent. Mater.* **2007**, *23*, 1447–1459.